New Ultra-Wide Stopband Low-Pass Filter Using Transformed Radial Stubs

Kaixue Ma, *Senior Member, IEEE*, and Kiat Seng Yeo

***Abstract*—A new type of low-pass filter (LPF) with ultra-wide band rejection and compact size by using a proposed transformed radial stubs (TRSs) is introduced and investigated. The operating mechanism of the filter is investigated based on proposed equivalent-circuit model. The implemented LPF with 1-dB cutoff frequency f_c of 3 GHz demonstrates stopband rejection up to $8f_c$ i.e., 24 GHz. The skirt selectivity is achieved up to −144 dB per octave through multiple-zero generation using TRSs. The measured passband insertion loss is less than 1.5 dB. I/O loading cells are used to further extend the deep stopband to more than $13f_c$ i.e., above 40 GHz. The size of the four-cell LPF is only $0.31\ \lambda g \times 0.24\ \lambda g$, ($\lambda g$ is the guide wavelength at center cutoff frequency) without using any lumped elements.**

***Index Terms*—Hairpin resonator, low-pass filter (LPF), microstrip, physically based lumped element model, radial stub, transformed radial stub (TRS), ultra-wideband (UWB).**

I. Introduction

LOW-PASS filters (LPFs) are widely used to remove undesired harmonics or spurious signals of the mixing products in the RF front-end circuits. The LPF with wide stopband and high stopband rejection is important to achieve the linearity of the front-end and to reduce the bit error rate (BER) of the high data-rate communication systems [1]–[7]. For example, the millimeter-wave receiver need to down-convert the RF signal to L-band signal for the baseband process. A good LPF is needed to suppress the mixed frequency elements and leakages of RF and local oscillator (LO) from the mixer [2], which may significantly degrade the receiver signal over noise ratio and linearity. A stepped-impedance LPF and open-stub LPF [1] are commonly used for LPF implementation, but these types of LPFs have a gradual cutoff response. Several techniques for the LPF designs have been reported to cope with this problem. In [6], an LPF employing a semilumped element composed of a lumped capacitor and a section of transmission line was proposed. The use of the multiple lumped elements will increase component and assembling cost, especially in the high RF frequency range, where the elements are expensive than their counterparts in lower frequency. Multisection LPFs using microstrip elements such as interdigital capacitors [1], coupled lines [4], [5], and stepped-impedance hairpin resonators [6]–[9] are the other effective approaches. The merits of stepped-impedance hairpin resonators are relatively smaller size and additional zeros in the stopband achieved through an additional electric coupling path. Recently, defected ground structure (DGS) usage in the LPFs for wide stopband has been demonstrated [10], [11]. However, the DGS for the microstrip line bring the disadvantages [12] of the additional radiation due to the partially open ground. A structure [13], [14] using a single quarter-wavelength resonator with one section of anticoupled lines with short circuits at one end can be used as a wide stopband LPF, but the stopband bandwidth, rejection depth, and selectivity are not enough for some applications like a millimeter-wave receiver.

In this paper, instead of using DGS, stepped-impedance or open stub, we design an LPF with a planar configuration and free of lumped *RLC* elements for low-cost and high-performance applications. A new low-pass configuration using transformed radial stubs (TRSs), which is formed by the coupled line transformer connected with a radial stub (the radial stub has intrinsic wide stopband characteristics as demonstrated in [14]–[16]) in shunt, is proposed and investigated to achieve a unique planar nonlumped-element LPF with steep rolloff, ultra wide stopband, compact size, and low cost simultaneously. By using the proposed physically based lumped element model, the operating mechanism of the LPF is investigated. The proposed LPFs demonstrate an ultra-wide stopband up to $8f_c$. Furthermore, a novel compact loading cell (LC) in I/O is introduced to further extend the stopband of the proposed LPF. With I/O LCs, the stopband of the proposed LPF is further extended to above 40 GHz, i.e., $13f_c$ with stopband rejection of more than 30 dB. The packaging effect, which is a challenge for wideband design, is also investigated.

This paper is organized as follows. In Section II, the proposed TRS is introduced with its equivalent-circuit model. The equivalent physical model and its parameters of the unit TRS is derived from the transmission line models. In Section III, the proposed LPF through cascading of multiple TRS cells is investigated and designed. Both theoretical and experimental results are presented. In Section IV, an LC in I/O ports is introduced and investigated to further extend the stopband of the multiple-cell TRS LPF. In Section V, the packaging effects are investigated based on experiment. Finally, this paper is concluded in Section VI.

Manuscript received September 26, 2010; revised October 21, 2010; accepted October 30, 2010. Date of publication December 20, 2010; date of current version March 16, 2011. This work was supported by the ST Electronics and Defence Science and Technology Agency (DSTA), Singapore. This paper is an expanded paper from the IEEE MTT-S Int. Microwave Symposium, Anaheim, CA, May 23–28, 2010.

The authors are with the Electrical and Electronic Engineering School, Nanyang Technological University, Singapore 609602 (e-mail: kxma@ieee.org; eksyeo@ntu.edu.sg).

Color versions of one or more of the figures in this paper are available online at http://ieeexplore.ieee.org.

Digital Object Identifier 10.1109/TMTT.2010.2095031

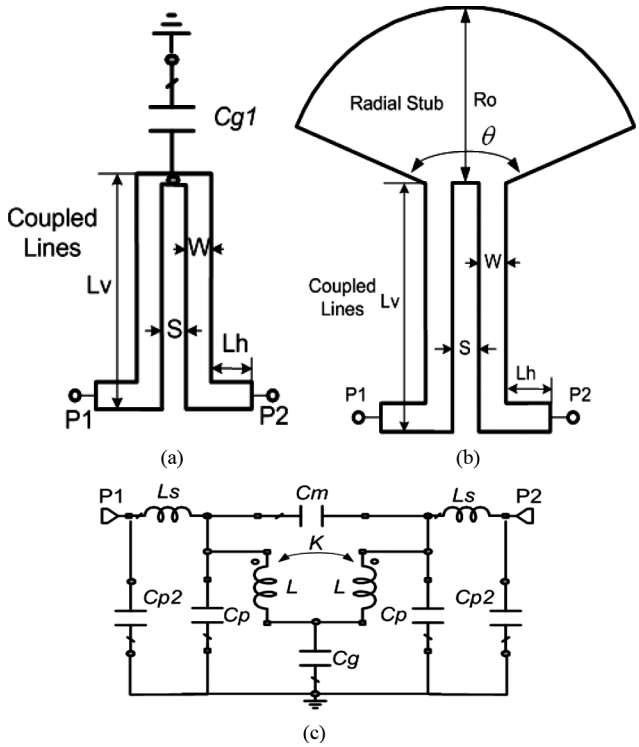

Fig. 1. Proposed lumped element cells and their equivalent-circuit model. (a) Transformer with lumped shunt capacitor. (b) Transformer with radial stub. (c) Equivalent-circuit model of (a) and (b).

II. Modeling of Unit LPF Cell

The physical model is useful to understand and investigate the operating mechanism of the microwave structure and circuits [1]. Fig. 1 shows the proposed TRS unit LPF cell and its equivalent-circuit model. Both of the structures in Fig. 1(a) and (b) could be equivalent to the circuit model, as shown in Fig. 1(c), under the constraint of the elements inside, and the capacitance of $Cg1$ in Fig. 1(a) would be lumped capacitor or other capacitance circuits like straight stub or radial stub. In the following, we will derive the model of the unit cell from the transmission line elements and then investigate the unique characteristics of the proposed LPF cell based on the proposed model.

A. Element Model

Fig. 2(a) shows the parameters of a four-port distributed coupled-line section, which can be modeled as a lumped element model, as shown in Fig. 2(b) approximately, when the electrical length is less than a quarter-wavelength. The values of the lumped elements in Fig. 2(b) can be derived by equating the two networks [13].

The values for L, K, and Cp in terms of Zoe, Zoo, and Lv are calculated as follows:

$$L = \frac{(Zoe + Zoo)\sin(\beta Lv)}{4\pi f} \tag{1}$$

$$Cp1 = \frac{\tan\left(\frac{\beta Lv}{2}\right)}{2\pi f Zoe} \tag{2}$$

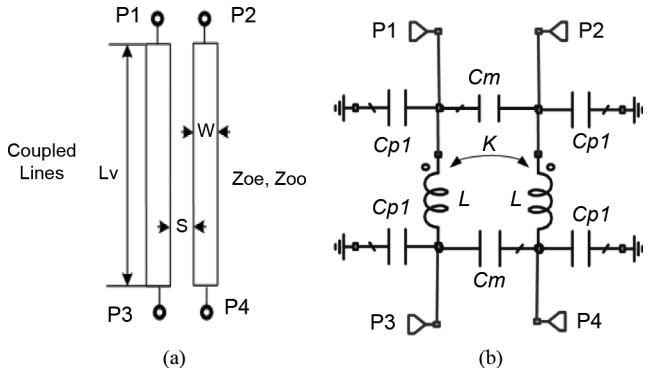

Fig. 2. Coupled lines and its equivalent-circuit model. (a) Four-port coupled lines. (b) Four-port equivalent-circuit model.

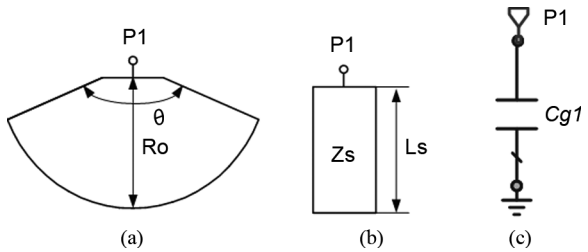

Fig. 3. Configuration of the capacitive elements. (a) Radial stub. (b) Straight stub. (c) Equivalent circuit of (a) and (b).

$$Cm = \left(\frac{1}{Zoo} - \frac{1}{Zoe}\right)\frac{\tan\left(\frac{\beta Lv}{2}\right)}{4\pi f} \tag{3}$$

$$k = \frac{Zoe - Zoo}{Zoe + Zoo}. \tag{4}$$

Fig. 3 shows two types of capacitive elements of the radial stub and straight stub and their equivalent circuit. The parameters of a distributed stub section, which include radial and the straight stubs in Fig. 3(a) and (b), respectively, can be approximately modeled as a lumped element, as shown in Fig. 3(c), under the constraint of the effective electric length smaller than a quarter-wavelength.

The capacitance of the radial stub can be extracted through one port S-parameter using (5) and (6)

$$Cg1 = \frac{-1}{2\pi f(\mathrm{imag}(Z\mathrm{in}))} \tag{5}$$

where $Z\mathrm{in}$ can be calculated as

$$Z\mathrm{in} = 50\left[\frac{(1+S11)}{(1-S11)}\right]. \tag{6}$$

For the straight stub, the equivalent capacitance can be directly derived as (7) when the effective electric length is less than a quarter-wave length

$$Cg1 = \frac{\tan(\beta Ls)}{2\pi f Zs}. \tag{7}$$

A section of distributed transmission line in Fig. 4(a) can be generally modeled as a lumped element model, as shown in Fig. 4(b), under the constraint of the effective electric length of

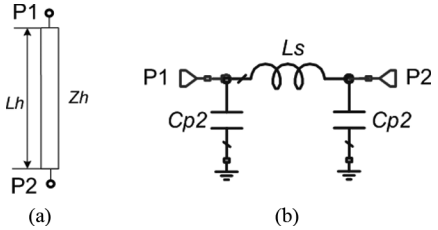

Fig. 4. Transmission line and its equivalent-circuit model. (a) Section of transmission line. (b) Equivalent circuit.

smaller than a quarter-wavelength. The values of the lumped element in Fig. 4(b) can be derived by equating the two networks as

$$Cp2 = \frac{1-\cos(2\beta L_h)}{2\pi f Z_h \cos(2\beta L_h)} \tag{8}$$

$$Ls = \frac{Z_h \sin(\beta L_h)}{2\pi f}. \tag{9}$$

B. Unit Cell Model and Characteristics

With the transmission line models, the structure in Fig. 1(b) can be treated as the cascading of the elements, as shown in Fig. 5(a). The major element values are given in (1)–(9). The other element values can be calculated as

$$Cp = Cp1 + Cp2 \tag{10}$$

$$Cg = 2Cp1 + Cg1. \tag{11}$$

The symmetrical physical based model, as shown in Fig. 5(b), can be analyzed through using the even- and odd-mode method. The even- and odd-mode equivalent circuits of the derived physical circuit model in Fig. 1(c) are given in Fig. 5(b) and (c), respectively. The even- and odd-mode admittances of the equivalent-circuit models can be calculated as

$$Y_{\text{ino}} = j\omega Cp2 + \cfrac{1}{j\omega Ls + \cfrac{1}{j\omega(Cp+2C_m) + \cfrac{1}{j\omega(L-L_m)}}} \tag{12}$$

$$Y_{\text{ine}} = j\omega Cp2 + \cfrac{1}{j\omega Ls + \cfrac{1}{j\omega Cp + \cfrac{1}{j\omega(L+L_m) + \cfrac{2}{j\omega Cg}}}} \tag{13}$$

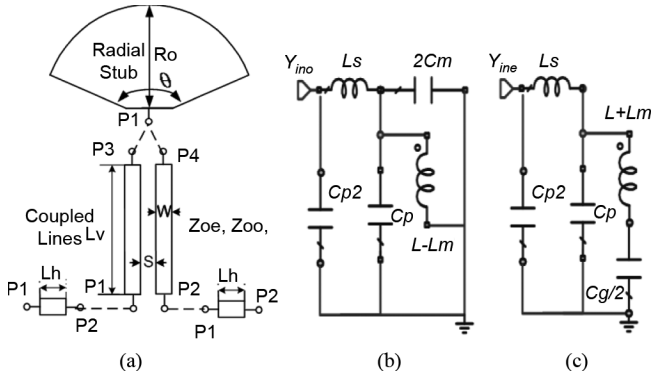

Fig. 5. Connections in LPF cell unit and its equivalent-circuit model in Fig. 1(c). (b) and (c) Odd- and even-mode circuits of Fig. 1(c). (a) Proposed unit LPF cell. (b) Odd-mode circuits of Fig. 1(c). (c) Even-mode circuits of Fig. 1(c).

where $Lm = k \times L$.

The S-parameter of the proposed equivalent circuits can be calculated through the odd- and even-mode admittances [1] as

$$S21 = \frac{Y_0 Y_{\text{ino}} - Y_0 Y_{\text{ine}}}{(Y_0 + Y_{\text{ine}})(Y_0 + Y_{\text{ino}})} \tag{14}$$

$$S11 = \frac{Y_0^2 - Y_{\text{ine}} Y_{\text{ino}}}{(Y_0 + Y_{\text{ine}})(Y_0 + Y_{\text{ino}})}. \tag{15}$$

The transmission zeros are generated when the even-mode admittance is equal to the odd admittance [1].

$$Y_{\text{ine}} = Y_{\text{ino}}. \tag{16}$$

By solving (16), the functions of the zeros of the proposed equivalent circuits can be calculated using (17) and (18), shown at the bottom of this page.

It is helpful to investigate an ideal lumped circuit model of the unit cell, which does not include the parameters of the transmission lines for understanding the operating mechanism of the idea circuit model. As shown in Fig. 6, the transmission responses of the idea circuit model according to different element values are compared. When $Lm = 0$, no zeros are generated in the stopband and the filter has a Chebshev response. When Lm and Cm are not equal zero, there are two zeros generated in the stopband. The increase of Lm will make the two zeros shift closer to the cutoff frequency. The zeros in stopband are dominantly determined by the magnetic coupling Lm of the transformer and electric coupling of Cm. The increase of Cm and Lm will decrease the cutoff frequency due to the mutual magnetic and elec-

$$f_{zp1} = \frac{1}{4\pi}\sqrt{-\frac{2(-2C_mL - C_gL_m + 2C_mL_m)}{C_gC_m(L^2-L_m^2)} - 2\times\sqrt{\frac{(-2C_mL - C_gL_m + 2C_mL_m)^2}{C_g^2C_m^2(L^2-L_m^2)^2}} - \frac{4}{C_gC_m(L^2-L_m^2)}} \tag{17}$$

$$f_{zp2} = \frac{1}{4\pi}\sqrt{-\frac{2(-2C_mL - C_gL_m + 2C_mL_m)}{C_gC_m(L^2-L_m^2)} + 2\times\sqrt{\frac{(-2C_mL - C_gL_m + 2C_mL_m)^2}{C_g^2C_m^2(L^2-L_m^2)^2}} - \frac{4}{C_gC_m(L^2-L_m^2)}} \tag{18}$$

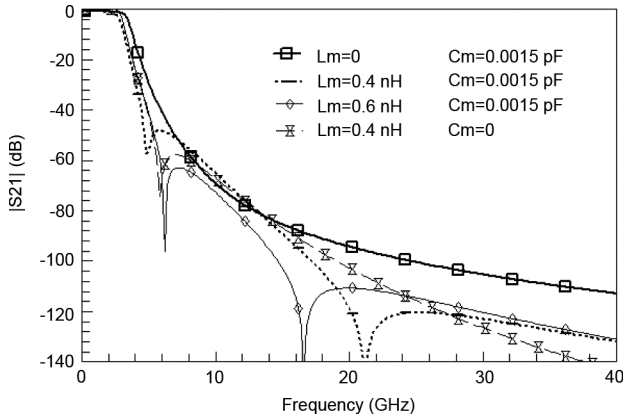

Fig. 6. Transmission characteristics of the ideal equivalent-circuit model. $Cp2 = 0.2$ pF, $Cp = 1.5$ pF, $L = 4.7$ nH, $Cg = 1.85$ pF, and $Ls = 1.36$ nH.

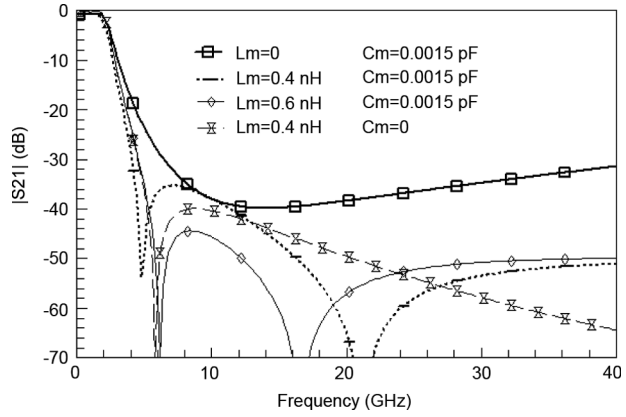

Fig. 7. Transmission characteristics of the ideal equivalent-circuit model. $Cp2 = 0.2$ pF, $Cp = 0.0001$ pF, $L = 4.7$ nH, $Cg = 1.85$ pF, and $Ls = 1.36$ nH.

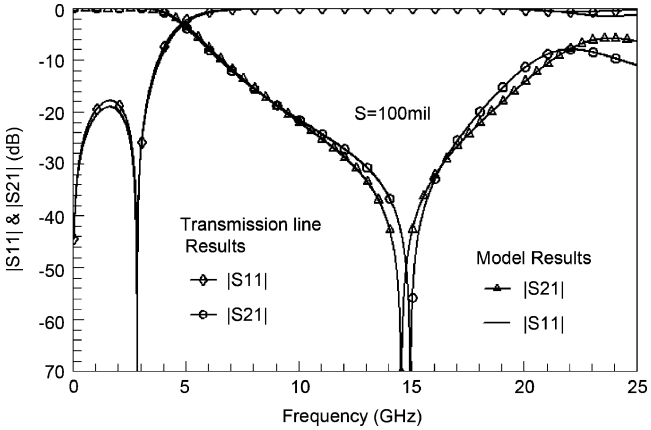

Fig. 8. Transmission and reflection characteristics of the unit cell in Fig. 1(d). $Ro = 113.4$ mil, $Lv = 172.4$ mil, $W = 6$ mil, $Lh = 15.9$ mil, and $\theta = 135°$.

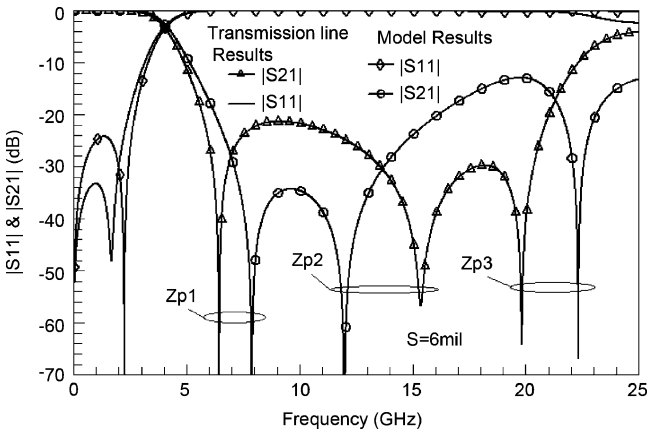

Fig. 9. Transmission and reflection characteristics of the unit cell in Fig. 1(d). $Ro = 113.4$ mil, $Lv = 172.4$ mil, $W = 6$ mil, $Lh = 15.9$ mil, and $\theta = 135°$.

tric coupling enhancement of the coupling elements to the main resonators composed by L and Cp (refer to even- and odd-mode equivalent circuits). Cp can affect the stopband rejection dominantly due to the parasitic resonance with Ls. The resonance of Ls and Cp may be in stopband or passband. If in the passband, as is the case in Fig. 6, additional poles can be generated in the passband and the stopband rejection is dramatically improved due to the increase of filter orders by two, i.e., from second order to fourth order. On the other hand, if resonance of Ls and Cp is in the stopband, as is the case in Fig. 7, the stopband rejection will be degraded with increase of Cp due to the resonance of Ls and Cp in the stopband. It is better to set resonance far from the interested stopband through choosing smaller values of Cp and Ls. The resonance of Ls and Cp in Fig. 7 is beyond the interested stopband, while the rejection depth is less than Fig. 6 due to the lower filter orders of two. The proposed equivalent-circuit model can be implemented by using the lumped elements according to the synthesized element values using (1)–(15) with the physical dimensions in Fig. 1(b), which are constraint conditions for the element value of the lumped circuit model in Fig. 1(c). A unit cell of the LPF is designed and investigated on the RO5880 with a dielectric constant of 2.2 and thickness of 10 mil. The simulation results based on a scalable lumped model and transmission line model are given in Figs. 8 and 9, respectively. It can be seen that the results of the physical-based lumped-element model agree with results of transmission line models when the coupling gap S is 100 mil. While when $S = 6$ mil, the passband agrees well with the transmission line model, but the locations of the zeros are different. The difference of the zero locations and depth in the higher frequency range is acceptable because of two reasons. Firstly, the equivalent lumped circuit model may beyond the constraint conditions in the high-frequency range where the electric length may be larger than a quarter-wave length and the high-order parasitic effects become dominant. Secondly, refer to the ideal model results in Figs. 6 and 7, the zeros in the stopband are quite sensitive to the value of Lm and Cm , especially for Cm. A smaller change of Cm by 0.0015 pF, the zeros change dramatically and make the model difficult to accurately represent the stopband zeros. However, through the investigation of the physical model, we can better understand the operation mechanism and the zero generation behind the physical structures of the proposed TRS LPF cell. As shown in Fig. 9, it is possible to generate three zeros in the stopband and the locations of these zeros can be controlled by the parameters of the coupled line and the radial

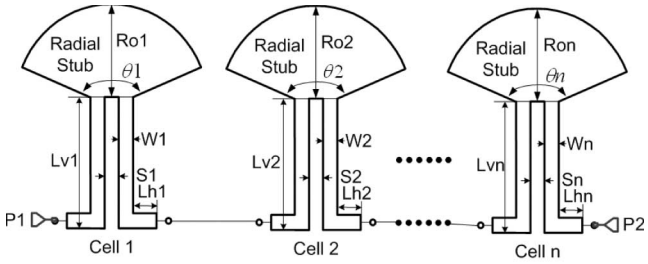

(a)

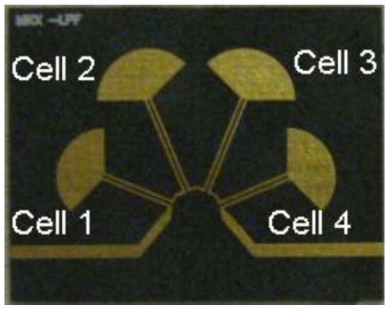

(b)

Fig. 10. TRS LPF configuration based on cascaded multiple TRS cells. (a) n-cell TRS LPF topology. (b) Four-cell TRS LPF structure.

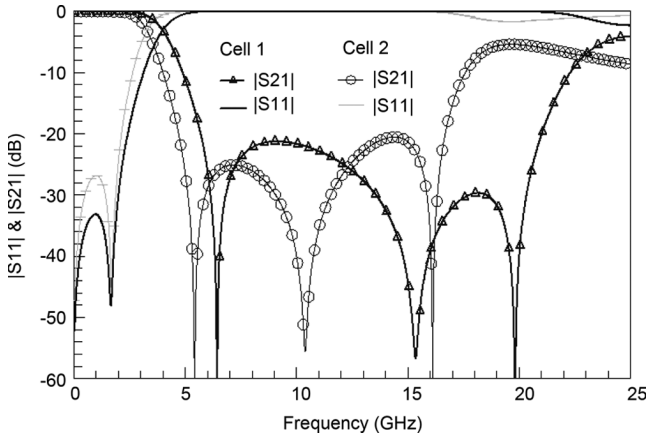

Fig. 11. Comparison of simulated characteristics of cell 1 and cell 2.

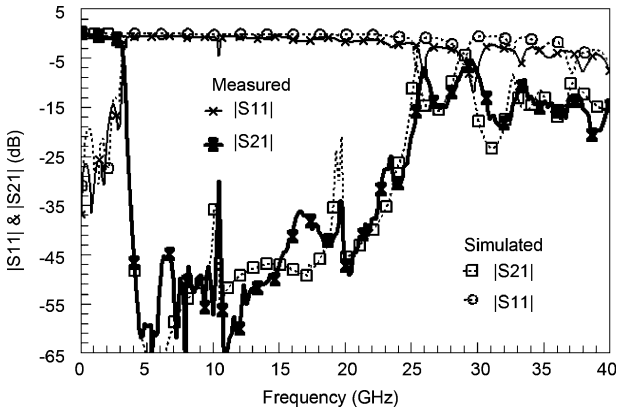

Fig. 12. Comparison of the simulation and experiment results of proposed four-cell TRS LPF in Fig. 10(b).

stub. One more zero of the TRS LPF is due to the intrinsic zero of radial stub compared to the lumped $Cg1$. The merits of this novel TRS cell can be seen clearly that the first zero ZP1 is good for the LPF to get a good rolloff in the close stopband, while ZP2 and ZP3 benefit the LPF in the upper stopband for wide and deep stopband rejection. This intrinsic zero generation mechanism of the proposed new low-pass cell gives advantages to control the stopband performance of the LPF.

III. TRS LPF Design

Though the single TRS LPF has intrinsic good stopband due to multiple zeros generated in stopband, the rejection depth and the skirt selectivity is still limited by the filter order, but this single TRS LPF can be used as a unit cell to form a high-order TRS LPF, which can dramatically improve the stopband skirt selectivity and rejection depth. As shown in Fig. 10(a), the TRS LPF unit can be cascaded up to n cells (n is an integer) to form a high-order filter using the network cascading [18] and [19]. The passband and stopband of the unit cell are designed according to the requirements of the filter specifications. If the deep stopband rejection and skirt selectivity are required, it is better to design the different cells with similar parameters to keep the stopband bandwidth similar to that of the unit cells while the rejection level is improved. If the wide stopband is needed, we can purposely design the different cells with different parameters that make the zeros allocated in the wide stopband range. The high-order TRS LPF is designed initially without considering the mutual coupling among the cells using the transmission line model. The full-wave electromagnetic (EM) simulator is then used to further optimize the design with considering the mutual coupling among the different cells.

A four-cell TRS LPF is designed as an example. To simply the design procedure, the four-cell LPF is designed to be symmetrical, i.e., cell 1 and cell 4 and cell 2 and cell 3 have the same dimensions, respectively. Thus, only two different cells need to be investigated and designed for the implementation of the four-cell LPF. The simulation results of cell 1 and cell 2 are compared in Fig. 11. The 1-dB cutoff frequencies of cell 1 and cell 2 are 3.4 and 2.9 GHz, respectively. The first zeros of cell 1 and cell 2 (in 6.46 and 5.44 GHz, respectively) are designed close to the passband to increase the skirt selectivity for the cascaded four-cell filter. Both cell 1 and cell 2 are designed to have three zeros in the stopband, which are attractive for the stopband rejection of the four-cell LPF. Cells 1–4 are cascaded, as shown in Fig. 10(b). The layout configuration is designed for compact size, physical locations of the cells, and better performance.

The simulated and measured results of the TRS LPF are compared in Fig. 12. Both results agree well in the passband and stopband. The filter has the cutoff frequency of 3 GHz, passband return loss (RL) greater than 12 dB, and stopband rejection better than 25 dB up to 24 GHz $(8f_c)$. From 4.1 to 10 GHz $(3.3f_c)$, the rejection is better than 45 dB. The skirt selectivity for the four-cell LPF is up to -144 dB per octave. The measured group delay in the passband is 0.6–1.2 ns, as shown in Fig. 13. The insertion loss (IL) is better than 1 dB in dc–2 GHz and better than 1.5 dB from dc to 3 GHz. The board sizes of the proposed planar LPF, shown in Figs. 10(b) and 14(a), is only 900 mil $\times$ 350 mil ($0.4\,\lambda g \times 0.155\,\lambda g$, λg is the guide wavelength at center cutoff frequency on the same substrate as the filters). Fig. 14(a)

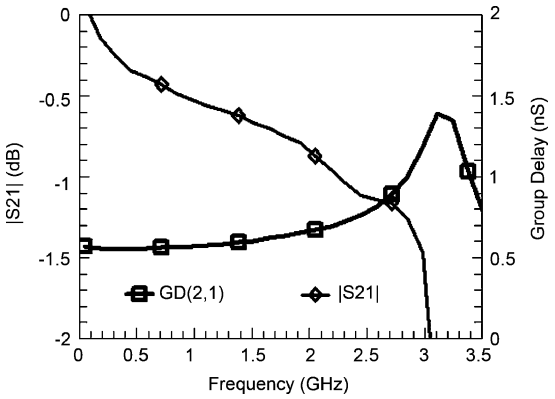

Fig. 13. Measured IL and group delay in the passband range of the TRS LPF in Fig. 10.

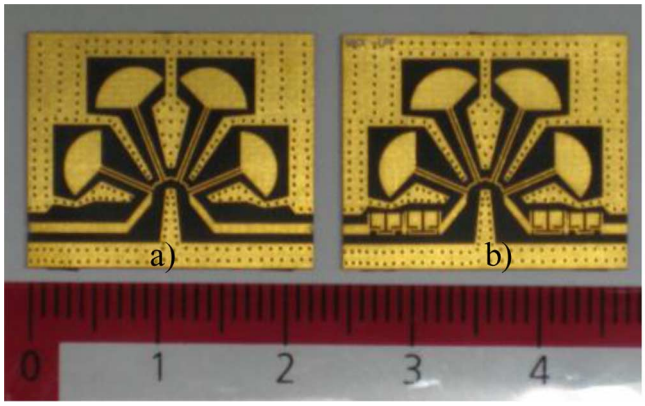

Fig. 14. Photograph of the fabricated filters TRS LPF for packaging with ruler for reference. (a) No LC. (b) With LCs.

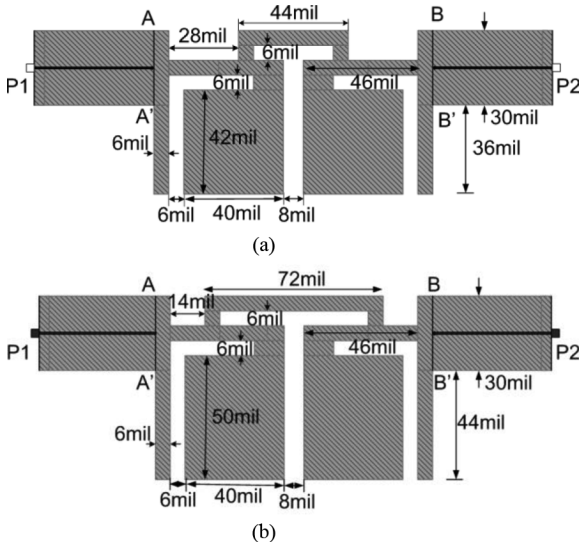

Fig. 15. Proposed LC structures for stopband extension. (a) LC1. (b) LC2.

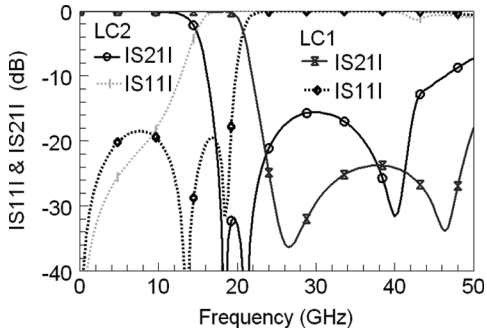

Fig. 16. Comparison of simulated results of LC1 and LC2.

is designed with ground shielding for packaging usage, as discussed in Section V. It is found that Fig. 14(a) has a similar frequency response as Fig. 10(b). The excellent rolloff or skirt selectivity filter is achieved by using the TRS LPF.

IV. Miniaturized I/O Loading for TRS LPF

To further extend the TRS LPF stopband while keeping the size as compact as possible, an LC structure is proposed as shown in Figs. 15(a) and (b). The stopband of the LC is purposely designed in the far stopband of the LPF, where the parasitic passband of the TRS LPF appears. Since the filter size is decreased with the increase of the cutoff frequency, the benefits of this approach are to achieve both wide stopband and compact size. The LCs are designed with high cutoff frequencies (13.5 and 20 GHz for LC2 and LC1, respectively) to achieve compact size. The stopband of LC1 and LC2 is designed with deep rejection in the TRS LPF parasite passband range. In Fig. 15, the LC characteristics are extracted through de-embedding from I/O ports (P1 and P2) to reference plane A-A' and B-B'. The simulated results of LC1 and LC2 are compared in Fig. 16. It is found that at least two zeros are generated, while keeping good matching and low IL below 7 GHz. The designed LCs, LC1 and LC2, are cascaded in each port of the two I/O ports as shown in Fig. 14(b). The TS LPF with LCs in Fig. 14(b) has the same board size as the filter in Fig. 14(a). The measured and the simulated results of the filter in Fig. 14(b) are compared in Fig. 17. Excellent agreement between the simulation and measurement are achieved below 15 GHz. The 1-dB cutoff frequency of Fig. 14(b) is close to that of the filter in Fig. 14(a). The filter in Fig. 14(b) has the 1-dB cutoff frequency f_c of 3 GHz and the RL in passband is improved to better than 12 dB. The 25-dB rejection band is extended from 24 GHz $(8f_c)$ for the filter in Fig. 14(a) toward more than 40 GHz $(13f_c)$ for the filter in Fig. 14(b). The simulated results are actually extended to 50 GHz $(16f_c)$, but the measurement is limited by test equipment in our laboratory. As the measured results shown in Fig. 18 for the filter in Fig. 14(b), the measured group delay, which is the key parameter for the high data rate or linearity communication system, is increased by 0.04 nS to 0.064–1.24 nS as compared with the results in Fig. 13 for the filter in Fig. 14(a). It can be seen that the LCs extend the stopband bandwidth dramatically while keeping the passband performance and the size almost the same as that of LPF without loading. The photograph of the filters with/without LCs is illustrated with the ruler in Fig. 14.

V. TRS LPF Packaging

For the LPF under wide passband or stopband operation, the packaging design is to be carefully designed to avoid any cavity modes [19] generated due to the packaging house. To avoid the mutual coupling among the different cells that may cause

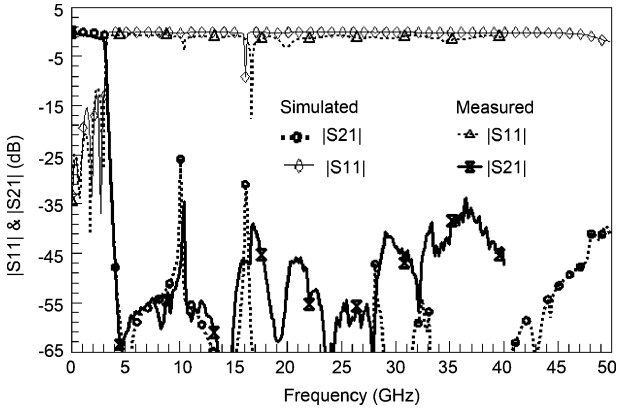

Fig. 17. Comparison of the simulation and experiment results of TRS LPF with LCs.

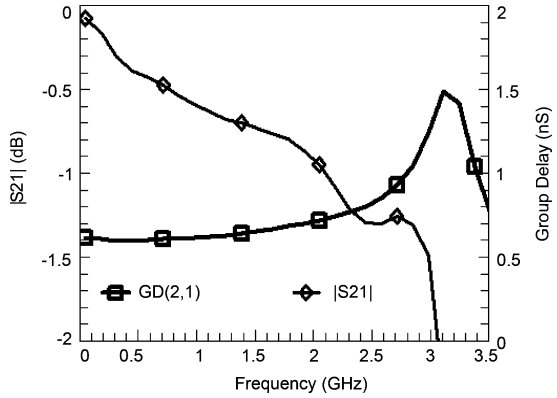

Fig. 18. Measured IL and group delay in the passband range of the TRS LPF with LCs.

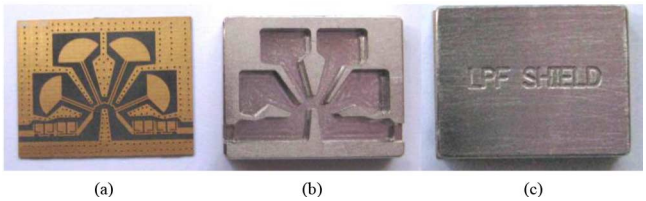

Fig. 19. Photograph for the TRS LPF packaging. (a) TRS LPF. (b) Cover. (c) Packaged LPF.

leakage modes and degrade the stopband performance of the TRS LPF in the packaging house, a top cover, which has six separate air cavities corresponding to the TRS cell 1-4 and the I/O LCs portions, each with height of 3 mm, is designed and fabricated as shown in Fig. 19(b). The conductive adhesive material is used to assemble the ground region to the metal wall of the top cover. The TRS LPF after assembling is shown in Fig. 19(c). For the TRS LPF with LC, the measured results of the LPF with and without packaging are compared in Fig. 20. The packaging house can improve the IL from 2 to 3 GHz around 0.1 dB. The stopband rejection is improved more than 3 dB in most of the stopband region. The RL in the whole frequency range is almost not affected by packaging. It can be seen that the proposed packaging structure actually improves the filter performance.

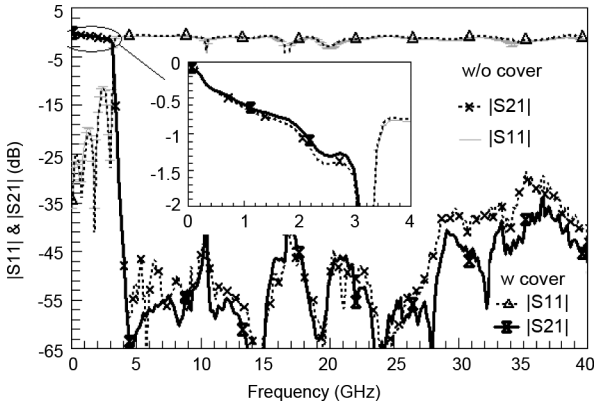

Fig. 20. Comparison of the experiment results of loading-cell TRS LPF with and without packaging house.

VI. Conclusion

In this paper, a new type of LPF by using TRSs was proposed and investigated using the physically based circuit model. The zero generation mechanism was investigated and used for stopband control. The LCs, which generate additional zeros in the far stopband of the TRS LPF, are used to further extend the stopband bandwidth of the TRS LPF. The measured results of the proposed filters demonstrate not only an ultra-wide stopband, deep stopband rejection, low IL, and compact size, but also good group delay and skirt selectivity. Most important is that the proposed high-performance planar filter structure does not require any lumped elements and this will be good for low-cost and high-yield applications.

Acknowledgment

The authors would like to thank the editors and reviewers of this Transactions for their valuable comments, which make this paper more readable.

References

[1] J.-S. Hong and M. J. Lancaster, *Microstrip Filters for RF/Microwave Applications*. New York: Wiley, 2001.
[2] A. Chu, W. E. Courtney, L. J. Mahoney, M. J. Manfra, and A. R. Colawa, "A dual function mixer circuit for millimeter wave transceiver applications," in *IEEE MTT-S Int. Microw. Symp. Dig*, 1985, pp. 120–123.
[3] M. Hayati and A. Lotfi, "Elliptic-function lowpass filter with sharp cutoff frequency using slit-loaded tapered compact microstrip resonator cell," *IET Electron. Lett.*, vol. 46, no. 2, pp. 733–736, Jan. 2007.
[4] W.-H. Tu and K. Chang, "Compact microstrip low-pass filter with sharp rejection," *IEEE Microw. Wireless Compon. Lett.*, vol. 15, no. 6, pp. 404–406, Jun. 2005.
[5] Y.-W. Lee, S.-M. Cho, G.-Y. Kim, J.-S. Park, D. Ahn, and J.-B. Lim, "A design of the harmonic rejection coupled line low-pass filter with attenuation poles," in *IEEE MTT-S Int. Microw. Symp. Dig*, 1999, pp. 682–685.
[6] L.-H. Hsieh and K. Chang, "Compact elliptic-function low-pass filters using microstrip stepped-impedance hairpin resonators," *IEEE Trans. Microw. Theory Tech.*, vol. 51, no. 1, pp. 193–199, Jan. 2003.
[7] J.-T. Kuo and J. Shen, "A compact distributed low-pass filter with wide stopband," in *Proc. Asia–Pacific Microw. Conf.*, 2001, vol. 1, pp. 330–333.
[8] L. Li, Z.-F. Li, and J.-F. Mao, "Compact lowpass filters with sharp and expanded stopband using stepped impedance hairpin units," *IEEE Microw. Wireless Compon. Lett.*, vol. 20, no. 6, pp. 240–242, Jun. 2010.

[9] J.-W. Sheen, "A compact semi-lumped low-pass filter for harmonics and spurious suppression," *IEEE Microw. Wireless Compon Lett.*, vol. 10, no. 3, pp. 92–93, Mar. 2000.
[10] G. M. Yang, R. Jin, J. G. X. Huang, and G. Xiao, "Ultra-wideband bandpass filter with hybrid quasi-lumped elements and defected ground structure," *IET Microw. Antennas Propag.*, vol. 1, no. 3, pp. 733–736, Jun. 2007.
[11] S.-W. Ting, K.-W. Tam, and R. P. Martins, "Miniaturized microstrip lowpass filter with wide stopband using double equilateral U-shaped defected ground structure," *IEEE Microw. Wireless Compon. Lett.*, vol. 16, no. 5, pp. 240–242, May 2006.
[12] Z. Du, K. Gong, J. S. Fu, B. Gao, and Z. Feng, "Influence of a metallic enclosure on the S-parameters of microstrip photonic bandgap structures," *IEEE Trans. Electromagn. Compat.*, vol. 44, no. 2, pp. 324–328, May 2002.
[13] M.-Y. Hsieh and S.-M. Wang, "Compact and wideband microstrip bandstop filter," *IEEE Microw. Wireless Compon. Lett.*, vol. 15, no. 7, pp. 472–474, Jul. 2005.
[14] R. Li, D. I. Kim, and C. M. Choi, "Compact structure with three attenuation poles for improving stopband characteristics," *IEEE Microw. Wireless Compon. Lett.*, vol. 16, no. 12, pp. 663–665, Dec. 2006.
[15] F. Giannini, R. Sorrentino, and J. Vrba, "Planar circuit analysis of microstrip radial stub," *IEEE Trans. Microw. Theory Tech.*, vol. 32, no. 12, pp. 1652–1655, Dec. 1984.
[16] R. Sorrentino and L. Roselli, "A new simple and accurate formula for microstrip radial stub," *IEEE Microw. Guided Wave Lett.*, vol. 2, no. 12, pp. 480–482, Dec. 1992.
[17] K. Ma and K. S. Yeo, "Novel low cost compact size planar low pass filters with deep skirt selectivity and wide stopband rejection," in *IEEE MTT-S Int. Microw. Symp. Dig*, 2010, pp. 233–236.
[18] J. Hogerheiden, M. Ciminera, and G. Jue, "Improved planar spiral transformer theory applied to a miniature lumped element quadrature hybrid," *IEEE Trans. Microw. Theory Tech.*, vol. 45, no. 4, pp. 543–545, Apr. 1997.
[19] K. Ma, J.-G. Ma, M. A. Do, and K. S. Yeo, "Experimentally investigating slow-wave transmission lines and filters based on conductor-backed CPW periodic cells," in *IEEE MTT-S Int. Microw. Symp. Dig*, 2005, pp. 1653–1656.
[20] K. Ma, J.-G. Ma, M. A. Do, and K. S. Yeo, "Characterizing and modeling conductor-backed CPW periodic band stop filter with miniaturized size," in *IEEE MTT-S Int. Microw. Symp. Dig*, 2007, pp. 983–986.

Kaixue Ma (S'05–M'05–SM'09) received the B.E. and M.E. degrees from Northwestern Polytechnical University, Xi'an, China, in 1997 and 2002, respectively, and the Ph.D. degree from Nanyang Technological University (NTU), Singapore, in 2007, all in electrical engineering.

From August 1997 to December 2002, he was with the China Academy of Space Technology (CAST), Xi'an, China, where he was Group Leader of the Millimeter-Wave Group focused on components and subsystems and inter-satellite link systems. From 2004 to 2005, he was involved with 60-GHz system and mixer designs with the Wireless Communication Laboratory, National Institute of Information and Communications Technology (NICT). From 2005 to 2007, he was with MEDs Technologies as a Research and Development Manager, where he performed design services and developed products for WiMAX equipment used by Agilent Malaysia and 10-Gb/s optical parallel transceivers test modules for AVAGO Singapore, etc. From 2007 to 2010, he was with ST Electronics, as a Research and Development Manager and Project Leader. He was also a Technique Management Committee member. He led a team successfully during the development of a 2–30-GHz ultra-wide bandwidth software-defined radio communication system. Since March 2010, he has been with NTU, as a Senior Research Fellow and Team Leader of the RF group of the 60-GHz flagship chipset project. He has authored or coauthored 50 papers. His research interests include software-defined radio, high-frequency circuits and system design using technologies like CMOS, monolithic microwave integrated circuits (MMICs), and microelectromechanical systems (MEMS). He holds two patents with five patents pending.

Dr. Ma is a technical reviewer for several prestigious international journals. He was the recipient of the Best Technical Paper Award of CAST in 2002.

Kiat Seng Yeo received the B.Eng. degree in electrical engineering (with honors) and Ph.D. degree in electrical engineering from the Nanyang Technological University (NTU), Singapore, in 1993 and 1996, respectively.

In 1996, he joined the School of Electrical and Electronic Engineering, NTU, as a Lecturer. He is a widely known authority on low-power integrated circuit (IC) design and a recognized expert in CMOS technology and RF IC design. He was the first person in South East Asia to set up a facility to perform research and development in RF CMOS device modeling and characterization. His research achievements and contributions in IC design have been recognized in both academic and industry. As a result of his innovative pioneering work in the field of IC design, he has successfully attracted more than S$30 million of external research funding from various funding agencies and industry over the last five years. Since 1996, he has provided consultation services to statutory boards, local Society of Manufacturing Engineers (SMEs) and multinational corporations in the areas of IC design. Several of his patents were licensed to companies for commercial exploitation. He authored *Intellectual Property for Integrated Circuits* (J. Ross Publishing, 2009, Int. Ed.), *Design of CMOS RF Integrated Circuits and Systems* (World Sci., 2009, Int. Ed.), *Low-Voltage, Low-Power VLSI Subsystems* (McGraw-Hill, 2005, Int. Ed.), *Low-Voltage Low-Power Digital BiCMOS Circuits: Circuit Design, Comparative Study, and Sensitivity Analysis* (Prentice-Hall, 2000, Int. Ed.), and *CMOS/BiCMOS ULSI: Low-Voltage, Low-Power* (Prentice-Hall, 2002, Int. Ed.). The latter was translated to Chinese and was one of the excellent foreign textbooks in China. He has also authored or coauthored three book chapters and over 300 international journal and conference papers. He holds 25 patents, including two patents for the world's smallest integrated transformer. He is the inventor of several high Q-factor RF spiral inductors and co-inventor of quite a few novel circuit techniques for RF IC applications. With his exemplary research leadership and several major breakthroughs in the field of IC design, NTU was ranked 16th in the world and among the top three in Asia in 2008 Integrated Circuit Design Research Ranking for Worldwide Universities published by the *Journal of Circuits, Systems and Computers*. He has supervised or trained over 100 researchers and postgraduate students, many of whom had become successful leaders in industry and academia. He has also contributed significant services to NTU and professional societies. He was Sub-Dean (Student Affairs), Program Manager of the System-on-Chip Flagship Project, Research Coordinator of the Integrated Circuit Design Group, and Principal Investigator of the Integrated Circuit Technology Group, NTU. In 2009, he founded VIRTUS, a S$50 million IC Design Centre of Excellence jointly funded by NTU and Singapore's Economic Development Board. He is currently a board member of the Singapore Semiconductor Industry Association (SSIA) and Head of the Division of Circuits and Systems.

Dr. Yeo has given several keynotes and invited presentations at various scientific meetings, workshops, and seminars. He serves on the Editorial Board of the IEEE TRANSACTIONS ON MICROWAVE THEORY AND TECHNIQUES. He holds or has held key positions in many international conferences as general chair, co-general chair, and technical chair. He was the recipient of the Public Administration Medal (Bronze) on National Day 2009 by the President of Singapore. He was also the recipient of the Distinguished Nanyang Alumni Award in 2009 for his outstanding contributions to the university and society.